Metallurgical and Materials Transactions A
41 (2010) 397-408

Influence of Al on the microstructural evolution and mechanical behavior of low carbon, manganese transformation-induced plasticity steel

Dong-Woo Suh[1]*, Seong-Jun Park[2], Tae-Ho Lee[2], Chang-Seok Oh[2] and Sung-Joon Kim[2]

[1]Graduate Institute of Ferrous Technology (GIFT), Pohang University of Science and Technology (POSTECH), Pohang, 790-784 Korea

[2]Structural Materials Division, Korea Institute of Materials Science Changwon, Kyungnam, 641-010 Korea

* Corresponding author

Tel: +82-54-279-9030, Fax: +82-54-279-9299

Email: dongwoo1@postech.ac.kr

Abstract

Microstructural design with Al addition is suggested for low carbon, manganese transformation-induced plasticity (Mn TRIP) steel for application in the continuous annealing process. With Al content of 1 mass%, the competition between recrystallization of the cold-rolled microstructure and the austenite formation cannot be avoided during intercritical annealing, and the recrystallization of the deformed matrix does not proceed effectively. Addition of 3 mass% Al, however, allows nearly complete recrystallization of the deformed microstructure by providing a dual-phase cold-rolled structure consisting of ferrite and martensite and suppressing excessive austenite formation at higher annealing temperature. An optimized annealing condition results in the room temperature stability of the intercritical austenite in Mn TRIP steel containing 3 mass% Al to permit persistent transformation to martensite during tensile deformation. The alloy presents an excellent strength-ductility balance combining a tensile strength of about 1GPa with a total elongation over 25%, which is comparable to that of Mn TRIP steel subjected to batch-type annealing.

1. Introduction

TRansformation Induced Plasticity (TRIP) steel is a representative high strength steel which utilizes phase transformation to control the mechanical properties [1-5]. Strain-induced martensitic transformation of metastable austenite plays a major role in improving the mechanical balance (Tensile strength × Elongation) enabling for TRIP steel to be actively applied in automotive industry. Nowadays, the tensile strength of commercially produced TRIP steel reaches about 1000MPa. However, when the tensile strength exceeds 800MPa, the elongation tends to decrease to less than 15% and the mechanical balance is significantly deteriorated [6-7]. Recently, Matlock et al. suggested a guideline for improving the mechanical balance of higher strength multiphase steel taking into account the characteristics of constituting phases [8]. They emphasized that a microstructural control ensuring higher stability as well as sufficient fraction of austenite would be essential to obtain higher tensile strength with desirable elongation.

Low carbon, manganese TRIP steel (Mn TRIP steel) based on an alloy system of Fe-0.1C-5Mn was first introduced by Miller [9]. Retained austenite fraction of 20~40% with optimized stability made it possible to exhibit an excellent mechanical balance after intercritical annealing. However, a prolonged heat treatment using batch-type

annealing process was required to obtain the desired properties and thus the more modern continuous annealing conditions were not tested [9-12]. In the present study, we investigated the influence of Al on the microstructural evolution and mechanical behavior of Mn TRIP steel using the continuous annealing process in order to obtain an exceptional mechanical balance. Mn TRIP steels with different Al content are prepared and heat-treated under continuous annealing conditions. The recrystallization of cold-rolled structure consisting of martensite or ferrite, and the formation of austenite during intercritical annealing are investigated, and the mechanical behavior of annealed sheets is examined with respect to the fraction and stability of retained austenite.

2. Microstructural design using Al addition

The microstructure of conventional TRIP steel consists of polygonal ferrite, bainitic ferrite and retained austenite. This microstructure is obtained by means of a two-step heat treatment including intercritical annealing and austempering. During the intercritical annealing, recrystallization of the cold-rolled microstructure and the reverse transformation to austenite occur. Epitaxial ferrite and bainitic ferrite start to form during rapid cooling and austempering, which enriches austenite with carbon, and thereby establishes the thermal stability of retained austenite during the final cooling to

room temperature [13]. In conventional TRIP steels, the large uniform deformation resulting from the strain-induced martensitic transformation of austenite contributes to the improvement of the mechanical balance. The recrystallization of ferrite, however, is also important to obtain a desirable mechanical balance because the ferritic matrix phase is subjected to a considerable amount of strain during deformation.

Meanwhile, in Mn TRIP steel, the enhanced hardenability of intercritical austenite due to its higher Mn content makes it difficult to control the fraction and stability of the austenite by a subsequent heat treatment following the intercritical annealing. This implies that it is necessary to achieve the specific characteristics of the austenite in the course of the single-step heat treatment of intercritical annealing. Mn additions substantially lower the temperature for the initiation of austenite formation during heating (A_s). Accordingly, when Mn TRIP steel is annealed at a sufficiently high temperature at which recrystallization can be completed in a short time, the fraction of reversely transformed austenite drastically increases and it becomes difficult to achieve the required thermal stability of austenite during final cooling. To address this difficulty, annealing at a temperature below 650^{o}C was adopted in previous studies on Mn TRIP steels [9-12]. This approach permitted the control of the austenite fraction in the range of 20~30 vol-% with fine grain structure. The prolonged annealing time (> 1hr) was

required for the recrystallization of the cold-rolled microstructure and the partitioning of Mn between ferrite and austenite [10-12].

During typical continuous annealing processing, the annealing temperature is generally higher than that of batch-type annealing to complete the recrystallization of cold-rolled structure during the rapid heating and the short holding time. Controlling the fraction and stability of austenite formed at higher annealing temperatures will therefore be critical for the application of continuous annealing process to Mn TRIP steel. Fig. 1 shows the equilibrium phase fractions in the Fe-0.12C-5Mn-0.5Si alloy system as a function of the Al content. The calculation is performed with CALPHAD method [14] using modified database taking into account recent experimental results for the Fe-Mn-Al-C alloy system [15]. In the temperature range of 700~800^{o}C, where the recrystallization of cold-rolled structure is expected to occur actively, the calculated equilibrium fraction of austenite is 67~100% in the case of the Al-free steel. The equilibrium fraction of austenite gradually falls off as the Al content increases and it is found that the single austenite phase region disappears and that the equilibrium fraction of austenite can be reduced to 20~30% with the addition of 3 mass% Al. It represents that Al will suppress the excessive formation of austenite even at higher temperature applicable for continuous annealing of Mn TRIP steel. This also has a favorable effect

on the stability of intercritical austenite. The influence of Al on equilibrium phase fraction suggests that microstructure design with Al might be one of the ways to manipulate the characteristics of intercritical austenite in Mn TRIP steel. The microstructural control by Al addition is verified with following experimental procedures.

3. Experimental

Table 1 shows the chemical compositions of investigated alloys. Based on the Al-free Fe-0.12C-5Mn-0.5Si alloy system, L-Al (1 mass% Al) and H-Al (3 mass% Al) alloys were prepared. Vacuum induction-melted ingots with a dimension of 300mm × 150mm × 50mm were reheated to 1200^{o}C for 2hrs and hot-rolled with finishing temperature above 800^{o}C followed by air cooling to room temperature. The thickness of hot-rolled sheets was 4.5mm. They were pickled in a 10% HCl solution and then cold-rolled to 1mm in thickness. The cold-rolled sheets were annealed using an infrared heating furnace with heating and cooling rates of 10^{o}C/s. The intercritical annealing temperatures of 660, 720, 780^{o}C for L-Al alloy and 720, 780, 840^{o}C for H-Al alloy were chosen taking into account the calculated equilibrium austenite fraction. The holding time at each annealing temperature was 2 minutes. Light microscopic

observation was performed with a standard method using 2% nital solution. For microstructural characterization using a scanning electron microscope (SEM) equipped with an electron back-scattered diffraction (EBSD) attachment, the specimens were mechanically polished with colloidal silica suspension in final polishing stage. The step size for EBSD measurement was 0.05μm or 0.025μm depending on the scale of microstructure. Thin foils for transmission electron microscope (TEM) were chemically polished in a 10%HF+H_2O_2 solution to a thickness of 50μm and then electrolytically polished in a twin-jet polishing apparatus using a solution containing 15%$HCHO_4$+CH_3OH at -20^oC. The fraction of retained austenite was determined by XRD using Cu K_α radiation. Specimens were prepared by mechanical polishing followed by chemical polishing in a 10%HF+H_2O_2 solution. Integrated intensities of $(200)_\alpha$, $(211)_\alpha$, and $(220)_\gamma$, $(311)_\gamma$ reflections were used for the determination of the phase fractions of ferrite and austenite [16]. The uncertainty of austenite fraction with the XRD analysis is known to be around 5% of the evaluated one. It will be enlarged when the specimen has a preferred orientation which is not considered in the present study [17]. The mechanical properties of the annealed sheets were examined with a universal tensile testing machine using a crosshead speed of 2 mm/min. Sub-sized test coupons according to the ASTM [18] were used for the tensile tests.

4. Results

4-1. Microstructural evolution

Fig. 2 shows microstructures of hot-rolled sheets. The microstructure of the L-Al alloy mostly consists of martensite. It also contains a small fraction of white grains indicated with arrows, which are presumed to be ferrite. The microstructure mainly covered with martensite is ascribed to the high Mn content which increases the hardenability of the alloy considerably. For the H-Al alloy, the hot-rolled structure is a mixture of elongated ferrite and martensite. Given that the hot rolling was conducted in temperature range between 800~1200^{o}C, the calculated phase fraction in Fig. 1 (c) implies that the microstructure consists of austenite and ferrite during the hot rolling, which results in the elongated structure of ferrite and martensite after cooling. For steels with high Mn content, Mn segregation frequently occurs and has an influence on the microstructural evolution [19]. The Mn segregation possibly developed in the investigated alloys. In the banded structure of ferrite and martensite of H-Al steel, the ferrite and martensite will correspond to Mn lean and rich region, respectively, because Mn is austenite stabilizer and therefore the ferrite will preferentially form in Mn lean region. The EDS analysis shows that Mn content in ferrite is 5.5±0.2 mass% and that in martensite is 6.9±0.2

mass%, which confirms the non-uniform distribution of Mn. The Mn segregation will affect the microstructural evolution during subsequent process, which will be discussed later.

Figs. 3 and 4 give the microstructures of annealed sheets after cold-rolling observed with a light microscope. Recrystallized polygonal ferrite grains are hardly found in L-Al alloy for any annealing condition. Recovery is supposed to occur in the cold-rolled structure as an increase of annealing temperature, but it is not likely proceed actively at annealing temperature of 780^{o}C. It is believed to be related to re-transformation of austenite into fresh martensite during cooling from intercritical temperature. Meanwhile, recrystallized grains are observed in H-Al alloy for all annealing conditions. When annealed at 720^{o}C, recrystallization takes place in coarse ferrite (A) and fine grains presumed to be reversely transformed austenite are observed in regions formerly being martensite (B). It is noted that austenite grains evolve preferentially in Mn rich region. Increase of annealing temperature to 780^{o}C clarifies the newly transformed austenite grains, but further increase of annealing temperature to 840^{o}C introduces another phase (C), which is thought to be fresh martensite transformed from the intercritical austenite upon cooling.

Fig. 5 shows the retained austenite fraction in annealed sheets evaluated from XRD

profiles. In L-Al alloy, retained austenite fraction is 6% after annealing at 660^{o}C. It is considerably increased to 28% after annealing at 720^{o}C, and then decreased to 6% when annealed at 780^{o}C. The retained austenite fraction in the H-Al alloy can be preserved around 26~31% after annealing at temperatures of 720^{o}C and 780^{o}C, but it drops to 18% after annealing at 840^{o}C. Together with the microstructural observation, the dilatometric curves in Fig. 6 indicate that the change of the retained austenite fraction with the annealing temperature is associated with the martensite transformation. When martensite forms from austenite during cooling, the dilatometric curve deviates from the linear behavior due to the atomic volume difference between martensite and austenite [20]. The onset of deviation indicates the Ms temperature as indicated by arrow. The dilatometric curves in Fig. 6 reveal that the intercritical austenite is stable enough to resist martensite formation on cooling when annealed at 680^{o}C, 720^{o}C for L-Al alloy and 720^{o}C, 780^{o}C for H-Al alloy, but additional increments in annealing temperature lead to martensite formation in both alloys. The deterioration of thermal stability of intercritical austenite is believed to be connected with a lowering of the carbon content and a coarsening of austenite grains accompanied by rapid increase of the austenite fraction during the annealing at higher temperature. The more remarkable decrease of the austenite fraction in the L-Al alloy having a larger equilibrium austenite fraction at

the annealing temperature implies that the thermal stability of intercritical austenite is closely related to the fraction of austenite formed during annealing.

For detailed microstructure observations, EBSD analysis was performed on specimens containing comparable volume fractions of austenite after the heat treatment. The L-Al alloy annealed at 720^{o}C and H-Al alloy annealed at 720^{o}C and 780^{o}C has austenite fraction of 0.28, 0.26 and 0.31, respectively. Fig. 7 shows the phase mappings with boundary characteristics. In the L-Al alloy, fine austenite grains (FCC) reversely transformed during annealing can be distinguished. A considerable fraction of low-angle boundaries in the region indexed as BCC suggests that the recrystallization does not proceed effectively [21-22]. In contrast, the H-Al alloy exhibits completely recrystallized coarse ferrite grains with mostly high-angle boundaries. Small ferrite grains are also found in the region where fine austenite grains are formed. Some of them contain low-angle boundaries which indicate that the recrystallization is not completed in this region, but the overall microstructure indicates that the recrystallization of the cold-rolled microstructure is nearly completed. The dissimilar restoration processes of the cold-rolled structure in the L-Al and H-Al alloys lead to different boundary characteristics in the annealed sheets. The distribution of misorientation angles in Fig. 8 shows that 77.5% of boundaries in the L-Al alloy are low angle boundary ($0.5<\theta<15^{o}$).

The fraction of low angle boundary is only 43.8% in the H-Al alloy annealed at 720^{o}C and decreases further to 39.4% when annealed at 780^{o}C. A larger fraction of low angle boundary denotes a residual deformed microstructure and thus a sluggish progress of the recrystallization during annealing. Distribution of equivalent grain diameter of austenite and ferrite is presented in Fig. 9 and the average grain diameter is summarized in Table 3. The reversely transformed austenite grain has finer average diameter than ferrite grain as expected from the microstructural observation. It is noted that, even though a few ferrite grains have grain size around 5μm, the average diameter of ferrite grain is still evaluated to be submicron scale. That is because the average diameter is arithmetic mean not considering the area occupied by each grain. That is also why the duplex grain structure consisting of coarse and fine ferrite grain in the H-Al alloy is not clearly seen in the grain diameter distribution in Fig. 9.

Fig. 10 shows TEM micrographs and EDS analysis results for the Mn content of some austenite grains in the annealed sheets. The deformed structure on the right-hand side of Fig. 10(a) and the dislocation substructures in polygonal ferrite grains consistently indicate that the recrystallization occurs in a sluggish manner in L-Al alloy. Contrarily, the equiaxed grains with few dislocations suggest a nearly complete recrystallization in H-Al alloy. The average Mn content of 15 austenite grains is 6.2±0.8mass% in the L-Al

alloy and 7.2±0.4 mass% for 24 austenite grains in the H-Al alloy. Table 2 compares the nominal Mn content in the alloys, the calculated equilibrium Mn content at each annealing temperature and the measured ones. Mn contents in austenite do not reach levels corresponding to full partitioning. Furthermore, as mentioned, the Mn content in Mn-segregated region reaches 6.9 mass% in the H-Al alloy before annealing. It means that the redistribution of Mn during intercritical annealing is not so appreciable, which may come from the short annealing time.

4-2. Mechanical behavior

Average tensile properties of the annealed sheets are summarized in Table 4 and representative stress-strain curves are shown in Fig. 11. In L-Al alloy, the tensile strength is improved by increase of annealing temperature, but the yield strength has a minimum value at annealing temperature of 720^{o}C. After annealing at 660^{o}C and 720^{o}C, the microstructure consists of annealed martensite as matrix phase and reversely transformed austenite. Therefore, the yield strength will gradually decrease as an increase of annealing temperature due to the softening of matrix phase. But after annealing at 780^{o}C, a considerable amount of fresh martensite forms during cooling from intercritical temperature as indicated in the dilatometric curve in Fig. 6 (a) and it

contributes to the rebound of yield strength. Meanwhile, the tensile strength is not only influenced by the yielding but also affected by the work hardening which reflects the microstructural evolution during deformation. For the L-Al alloy, the increase of annealing temperature from 660^{o}C to 720^{o}C remarkably changes the work-hardening behavior. The notable work-hardening obtained after annealing at 720^{o}C is very likely due to the increase of austenite fraction shown in Fig. 5. This contributes to the improvement of the tensile strength by strain-induced transformation to martensite. The tensile behavior of specimen annealed at 780^{o}C does not exhibit a yield elongation but shows a rapid work-hardening with the highest tensile strength. It is analogous to that of commercial dual-phase steel. Given that the considerable amount of martensite forms upon final cooling in that annealing condition, a high density of mobile dislocation is introduced to accommodate the volume expansion around martensite. This accounts for the disappearance of the yield point elongation [20]. A similar tensile behavior is observed for the H-Al alloy annealed at 840^{o}C, which also allows martensite formation on final cooling. In the H-Al alloy, the yield strength decreases as the increase of annealing temperature. The major microstructural constituent is recrystallized ferrite after annealing of the H-Al alloy. More softening of ferrite with increase of annealing temperature is possibly associated with the change of yield strength. The H-Al alloy

annealed at 720°C does not show a notable work-hardening. Since the martensite formation has a primary effect on the work-hardening of steels containing the retained austenite, the little work-hardening even with an austenite fraction of 26% before deformation implies that the austenite is not likely to transform to martensite during tensile test. Meanwhile, the tensile behavior of the H-Al alloy annealed at 780°C is noteworthy because the mechanical balance is remarkably improved compared with those annealed in different conditions. Due to a persistent work-hardening along the deformation, it presents higher tensile strength than that annealed at 720°C even with lower yield strength. It is a characteristic feature of TRIP steel with austenite having proper mechanical stability. Tensile strength around 1GPa with total elongation over 25% is comparable to those reported in 0.1C-5Mn alloys subjected to a batch-type annealing [10-12]. It confirms that low carbon, manganese TRIP steel can be applied to the continuous annealing process while maintaining the mechanical balance by microstructural control with Al addition.

5. Discussion

Addition of 3% Al to low carbon, manganese TRIP steel permits both the recrystallization of the cold-rolled microstructure as well as the thermal stabilization of

austenite during typical continuous annealing processing. The alloy exhibits an excellent mechanical balance. The change of retained austenite fraction according to the Al content and annealing temperature shows that, as intended in microstructure design using Al, the austenite stability can be secured by suppressing excessive austenite formation at higher annealing temperature where the recrystallization of the deformed microstructure is completed in a short time.

As mentioned, the recrystallization behavior of cold-rolled structure is significantly influenced by the Al content. The recrystallized ferrite grains are rarely observed in the annealed L-Al alloy when observed by light microscopy and EBSD phase mapping. In addition, the polygonal ferrite grains found in TEM micrographs are frequently observed to have dislocation substructures. In contrast, the coarse and fine ferrite grains in the annealed H-Al alloy have equiaxed morphology and contain few dislocations. It reflects that the recrystallization in the H-Al alloy is almost completed even at the same annealing temperature. The difference in recrystallization behavior is thought to be attributed to the reduced competition between the recrytallization of cold-rolled microstructure and the reverse transformation to austenite as a result of the higher Al content. In the L-Al alloy, the austenite fraction is around 30% at an annealing temperature of 720^{o}C and it will increase rapidly at higher annealing temperatures. It

means that the recrystallization of the deformed microstructure and the austenite formation proceed simultaneously during intercritical annealing. Generally, the driving force for phase transformation is larger than that for recrystallization. From the calculation with CALPHAD method using Thermo-Calc software [14], the overall driving force for austenite formation is evaluated to be 152 J/mol at 720^{o}C and the driving force for nucleation of austenite is 1777J/mol for the L-Al alloy, which is quite larger than that for recrystallization, which is typically 10~100 J/mol [23]. Therefore, the formation of austenite in the deformed structure tends to encroach on the preferential nucleation sites for recrystallization and it also hinders the growth of recrystallized ferrite grains. Accordingly, the recrystallization will be retarded and proceed in a sluggish manner. On the other hand, the microstructure of cold-rolled H-Al alloy is separated into ferrite and martensite and thus the recrystallization of cold-rolled ferrite does not interfere with the austenite formation. Besides, in the region where cold-rolled martensite exists, the competition between the recrystallization and the reverse transformation will be mitigated because the equilibrium austenite fraction is less than that of the L-Al alloy. It suggests that the recrystallization in H-Al alloy will proceed more effectively.

As pointed by Matlock et al., the fraction and stability of retained austenite have

significant influence on the mechanical behavior of TRIP steels [8]. Fig. 5 indicates that austenite fraction around 30% can be obtained in both investigated alloys with appropriate annealing conditions. It has been reported that the stability of austenite depends on the grain size as well as chemical composition [24-26]. In particular, the effect of grain refinement becomes notable when the grain size is less than 1μm [24]. As mentioned, the average grain size of austenite in the annealed sheets is far below 1μm. Moreover, more than 90% of observed austenite grains have the size below 0.5μm as shown in the grain size distribution given in Fig. 9. Given that the M_s temperatures of the intercritical austenite calculated from the empirical equation taking into account the chemical effect of carbon and Mn [27] are 169^{o}C in the L-Al alloy annealed at 720^{o}C and 156^{o}C in the H-Al alloys annealed at 780^{o}C assuming a complete redistribution of carbon into austenite, both refinement and uniformity of austenite grain size are thought to have remarkable influence on the stabilization of austenite.

Fig. 12 presents the change of austenite fraction with apparent strain during tensile test. It is noted that the austenite fraction is evaluated from the different specimen deformed to each strain. In the H-Al alloy annealed at 720^{o}C, only 25% of initial austenite transforms to strain-induced martensite until the apparent strain reaches 15%. It implies that little work-hardening behavior in the stress-strain curve of that alloy is attributable

to the stability of austenite. Considering that the austenite in the H-Al alloy annealed at 720^{o}C has the smallest average grain size in the present study and that more than 98% of observed austenite grains are smaller than 0.5μm, the resistance against the strain-induced transformation to martensite would originate from the fine grain size of austenite. The stress-strain curve and the change of austenite fraction indicate that the austenite stabilized more than necessary can not provide persistent work-hardening and thus becomes ineffective to prevent a local deformation, which results in the deterioration of mechanical balance. Meanwhile, the L-Al alloy annealed at 720^{o}C and the H-Al alloy annealed at 780^{o}C have similar austenite fraction and grain size with comparable Mn content, but show quite different tensile behaviors in Fig. 11. It is associated with the dissimilar response of their retained austenite to the deformation as shown in Fig. 12. Compared with the retained austenite in the L-Al alloy of which 95% transforms to martensite upon apparent strain of 10%, the austenite in the H-Al alloy transforms gradually with deformation and 80% of initial austenite transforms to martensite when apparent strain becomes 25%, thus providing a continuous work-hardening and homogeneous deformation during tensile test. Nevertheless, it should be noted that the dissimilar response of austenite to the apparent strain does not necessarily reflects the difference in the intrinsic stability of austenite. That is because the

microstructure of the annealed steels are not the same for both alloys and thus the stress or strain exerted on the austenite grain will be different even at the same apparent strain. For example, fully recrystallized ferrite matrix as seen in the H-Al alloy will be in charge of a considerable amount of deformation, but lesser recrystallized matrix in L-Al alloy will not effectively cover the deformation and more stress or strain is possibly allocated to the austenite grains. Quantitative understanding of the different responses of austenite to the apparent strain even with similar morphology and chemical composition are thought to require a further investigation on a precise determination of the stress or strain allocated in individual phase during the deformation.

6. Conclusion

Low carbon, manganese TRIP (Mn TRIP) steel has superior mechanical balance to the conventional low carbon TRIP steels. In this study, we suggest a microstructure design based on Al additions for application of the continuous annealing processing rather than batch-type processing. The microstructural change after intercritical annealing and the mechanical behavior of the alloys containing of 1 mass% Al (L-Al) and 3 mass% Al (H-Al) are investigated and following conclusions can be drawn:

(1) The fraction of austenite formed during intercritical annealing can be controlled by means of Al additions to Mn TRIP steel. Al addition of 3 mass% limits the austenite fraction to 20~30 vol.-% at annealing temperatures in the range of 700^{o}C~800^{o}C, where recrystallization of deformed matrix actively proceeds.

(2) Appropriate annealing conditions for investigated alloys can stabilize the austenite formed during intercritical annealing. The average austenite grain size is around 0.22~0.29μm. In the L-Al alloy, recrystallization of the cold-rolled microstructure occurs in a sluggish manner due to the competition with the formation of austenite. Less interference between the recrystallization and the reverse transformation of austenite allows the rapid recrystallization of deformed structure in the H-Al alloy.

(3) The austenite fraction and stability is affected by the annealing condition and the Al content. Optimization of the austenite fraction and stability in the H-Al alloy can provide an excellent mechanical balance with a tensile strength around 1GPa and a total elongation in excess of 25% after continuous annealing processing.

References

[1] B.C. De Cooman: Curent Opinion in Solid State & Mater. Sci., 2004, vol.8, pp.285-303.

[2] J. Bouquerel, K. Verbeken and B.C. De Cooman: Acta Mater., 2006, vol.54, pp.1443-1456.

[3] S. Zaefferer, J. Ohlert and W. Bleck: Acta Mater., 2002, vol.52, pp.2765-2778.

[4] C. Jing, D.W. Suh, C.S. Oh, Z. Wang and S.J. Kim, 2007, vol.13, pp.13-19.

[5] C.P. Scott and J. Drillet: Scripta Mater., 2007, vol.56, pp.489-492.

[6] P. J. Jacques: Curent Opinion in Solid State & Mater. Sci., 2004, vol.8, pp.259-265.

[7] K. Sugimoto, M. Murata, T. Muramatsu and Y. Mukai: ISIJ Int., 2007, vol.47, pp.1357-1362.

[8] D.K. Matlock and J.G. Speer: Proceedings of the 3rd International Conference on Advanced Structural Steels, 2006, Gyengjoo, Korea, pp.744-781.

[9] R.L. Miller: Metall. Trans., 1972, vol.3, pp.905-912.

[10] T. Furukawa, H. Huang and O. Matsumura: Mater. Sci. & Tech., 1994, vol.10, pp.964-969.

[11] H. Huang, O. Matsumura and T. Furukawa: Mater. Sci. & Tech., 1994, vol.10, pp.621-626.

[12] H. Takechi: JOM, 2008, vol.60, pp.22-26.

[13] D.W. Suh, S.J. Park, C.S. Oh and S.J. Kim: Scripta Mater., 2007, vol.57, pp.1097-1100.

[14] Thermo-Calc Software, User's Guide, Version R.

[15] B.J. Lee, POSTECH, Pohang, Korea, Private communication, 2008.

[16] C. F. Jatczak: SAE Technical Paper Series 800426, 1980.

[17] B. C. Cullity: Elements of X-ray diffraction, Addision-Wesley, 1978, pp.517-518

[18] ASTM International, Designation E 8M – 03, 2003.

[19] S. W. Thompson and P. R. Howell: Mater. Sci. Technol., 1992, vol. 8, pp.777-784.

[20] D.W. Suh, S.J. Park and S.J. Kim: Metall. & Mater. Trans. A, 2008, vol.39A, pp.2015-2019.

[21] F. Heidelbach, H. R. Wenk, S. R. Chen, J. Pospiech and S. I. Wright: Mater. Sci. & Eng., 1996, vol.A215, pp.39-49

[22] F. J. Humphreys and M. Ferry: Mater. Sci. Technol., 1997, vol.13, pp.85-90.

[23] F.J. Humphreys and M. Hatherly: Recrystallization and related annealing phenomena, Pergamon, Oxford, 1995, pp.8-9.

[24] J. Wang and S.V.D. Zwaag: Metall. & Mater. Trans. A, 2001, vol.32A, pp.1527-1539.

[25] D.W. Suh, S.J. Park, C.H. Lee and S.J. Kim: Metall. & Mater. Trans. A, 2009, vol.40A, pp.264-268.

[26] S. Turteltaub and A.S.J. Suiker: Int. J. Solid and Structures, (2006), vol.43, pp.7322-7336.

[27] J. Mahieu, J. Maki, B. C. De Cooman and S. Claessens: Metall. & Mater. Trans. A, 2002, vol.33A, pp.2573-2580.

Table 1. Chemical compositions of investigated alloys (in mass%)

	C	Mn	Si	Al
L-Al	0.12	4.6	0.55	1.1
H-Al	0.12	5.8	0.47	3.1

Table 2. Mn content in austenitic phase (in mass%)

	Nominal	Equilibrium content at annealing temperature	Average of measured content
L-Al	4.6	7.6 (720^{o}C)	6.2
H-Al	5.8	8.8 (780^{o}C)	7.2

Table 3. Average equivalent diameters of austenite and ferrite grain from EBSD analysis (in μm)

	L-Al (720^{o}C)	H-Al (720^{o}C)	H-Al (780^{o}C)
Austenite	0.26	0.22	0.29
Ferrite	0.47	0.42	0.43

Table 4. Average tensile properties of investigated alloys

		YS (MPa)	TS (MPa)	U. El (%)	T. El (%)
L-Al	660^{o}C	936±1.9	988±2.9	11.5±0.6	16.7±1.7
	720^{o}C	766±2.9	1204±10.0	12.9±0.3	15.9±0.8
	780^{o}C	940±2.6	1461±6.4	6.2±0.2	8.6±1.3
H-Al	720^{o}C	814±4.3	854±2.5	14.7±1.2	21.7±3.9
	780^{o}C	714±13.3	994±10.4	23.8±0.8	27.5±1.1
	840^{o}C	444±3.7	1161±12.1	11.2±0.2	12.4±0.2

Figure 1. Equilibrium fraction of constituting phases in Fe-0.12C-5Mn-0.5Si alloy system containing (a) 0 mass% Al, (b) 1 mass% Al and (c) 3 mass% Al.

Figure 2. Optical micrographs of hot-rolled sheets for (a) L-Al alloy and (b) H-Al alloy.

Figure 3. Optical micrographs of cold-rolled L-Al alloy after annealing for 120s at (a) 660^{o}C, (b) 720^{o}C and (c) 780^{o}C.

Figure 4. Optical micrographs of cold-rolled H-Al alloy after annealing for 120s at (a) 720^{o}C, (b) 780^{o}C and (c) 840^{o}C.

Figure 5. Fraction of austenite retained after intercritical annealing. (Broken lines are equilibrium fraction and symbols are measured ones from XRD profiles)

Figure 6. Dilatometric curves upon cooling for intercritically annealed (a) L-Al alloy and (b) H-Al alloy.

Figure 7. EBSD phase mapping of (a) L-Al alloy annealed at 720^{o}C, (b) H-Al alloy at 720^{o}C and (c) H-Al alloy at 780^{o}C with indexing yellow phase as BCC and red phase as FCC. (Misorientation is between 2^{o}~15^{o} for purple line and more than 15^{o} for green line. Color image is available in the online article)

Figure 8. Distribution of misorientation angle in (a) L-Al alloy annealed at 720^{o}C, (b) H-Al alloy at 720^{o}C and (c) H-Al alloy at 780^{o}C.

Figure 9. Equivalent grain diameter distribution of ferrite and austenite in (a) L-Al alloy

annealed at 720^{o}C, (b) H-Al alloy at 720^{o}C and (c) H-Al alloy at 780^{o}C.

Figure 10. TEM micrographs of (a) L-Al alloy annealed at 720^{o}C and (b) H-Al alloy at 780^{o}C with Mn content in austenite grain.

Figure 11. Stress-strain curves of annealed sheets of (a) L-Al alloy and (b) H-Al alloy.

Figure 12. Change of retained austenite fraction with apparent strain during tensile test.

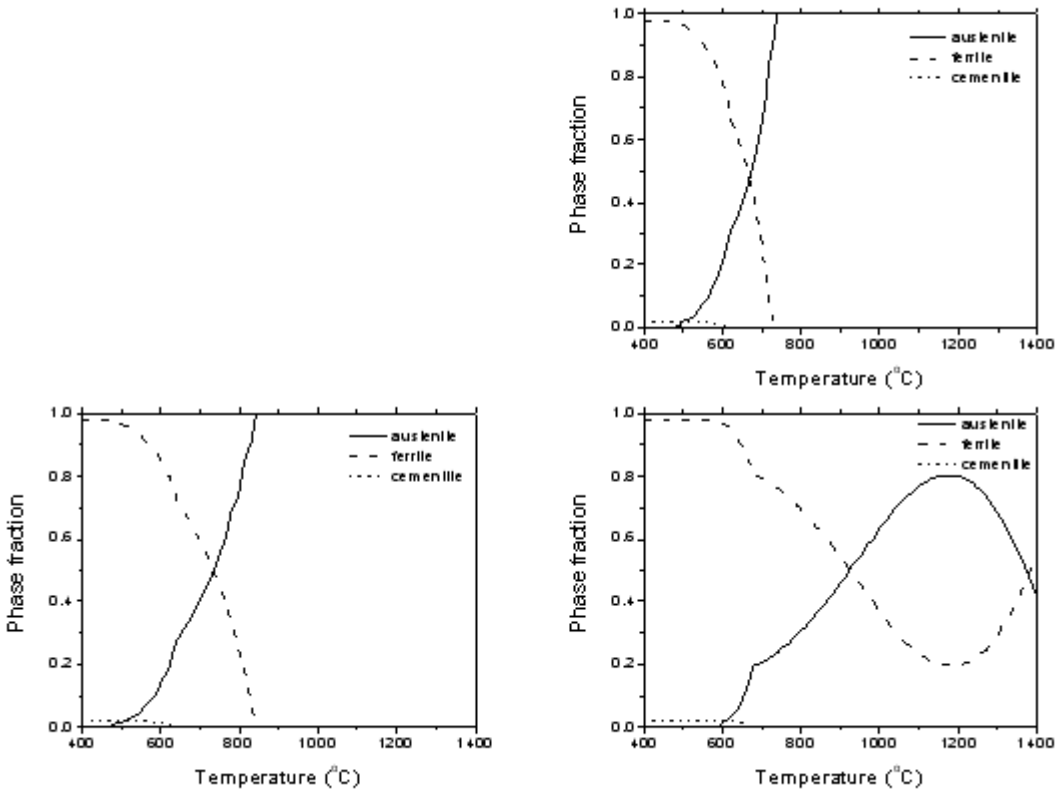
austenite
ferrite
cementite
Phase fraction
Temperature (°C)
1.0
0.8
0.6
0.4
0.2
0.0
400
600
800
1000
1200
1400

Fig. 1

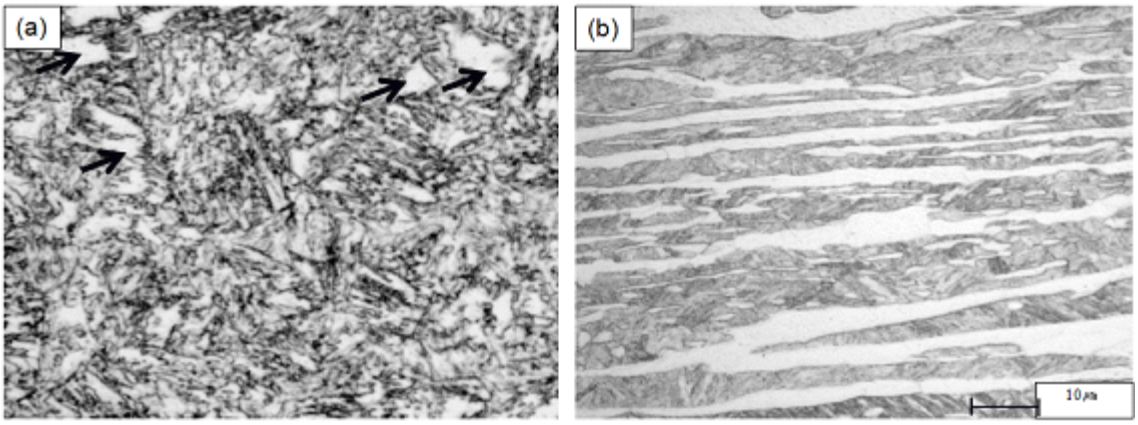

Fig. 2

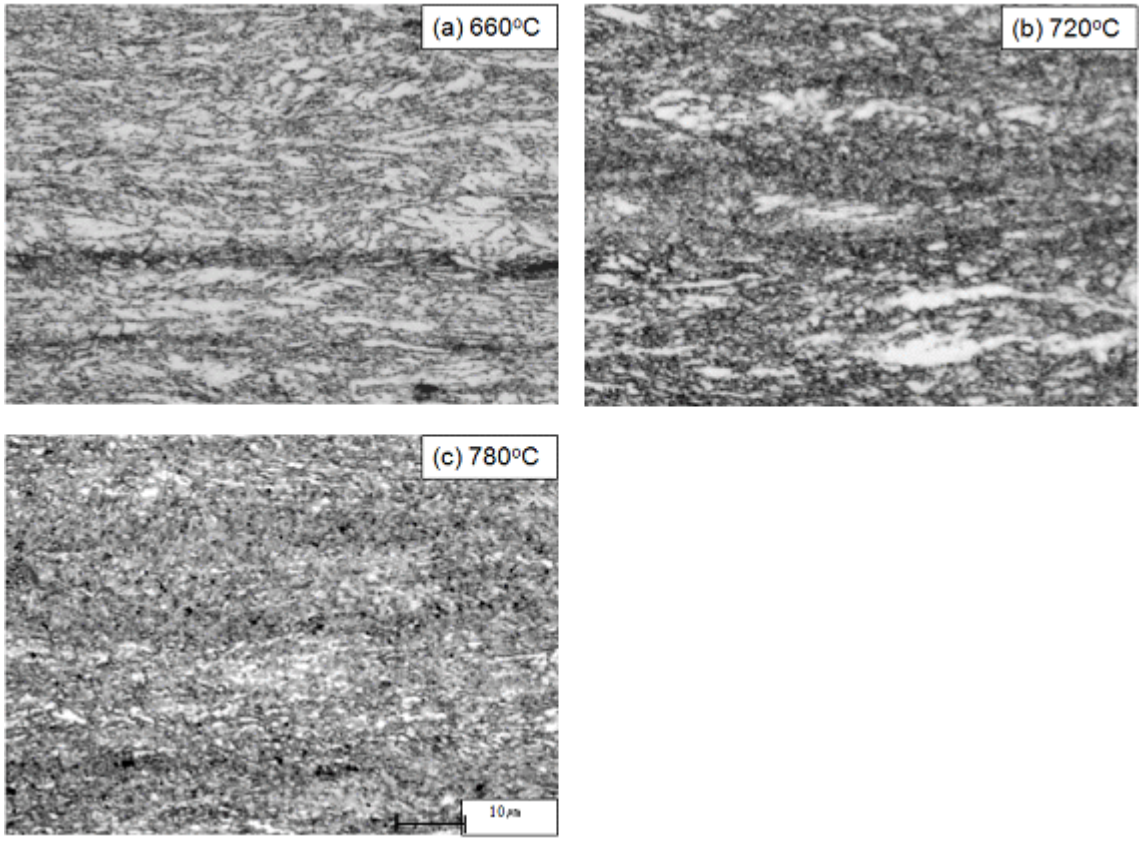

Fig. 3

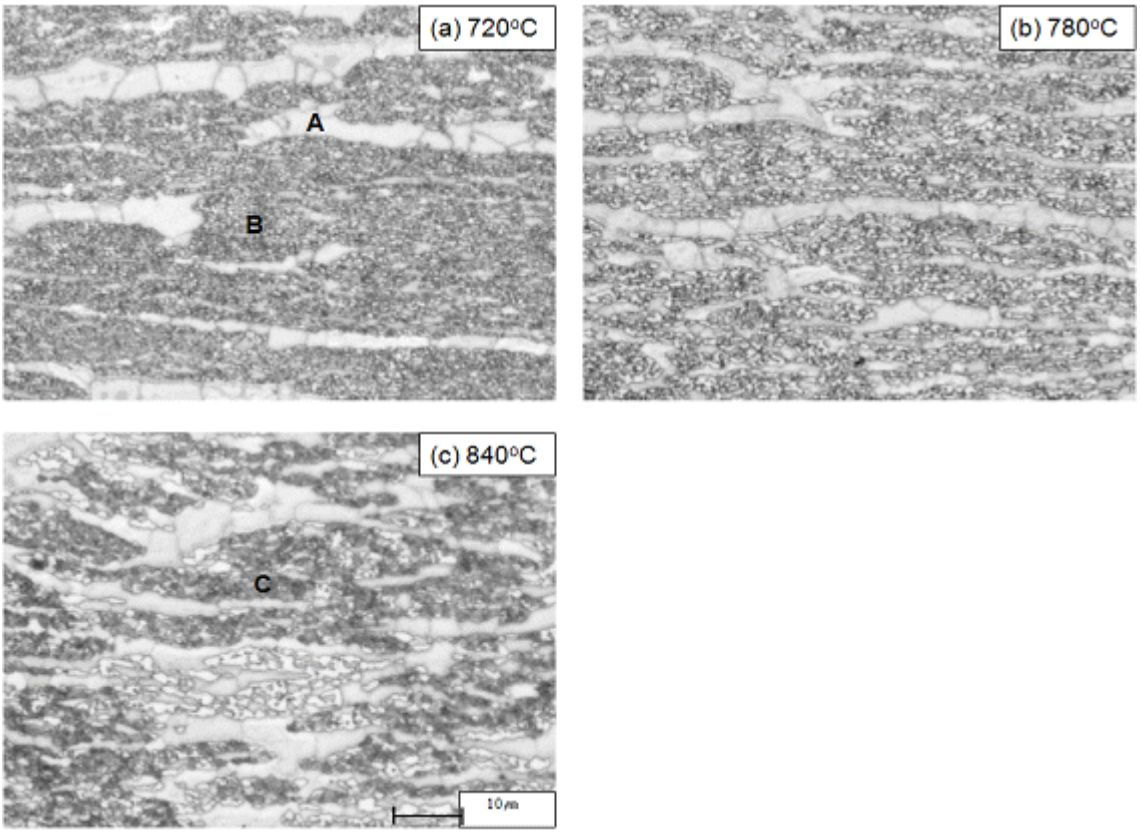

Fig. 4

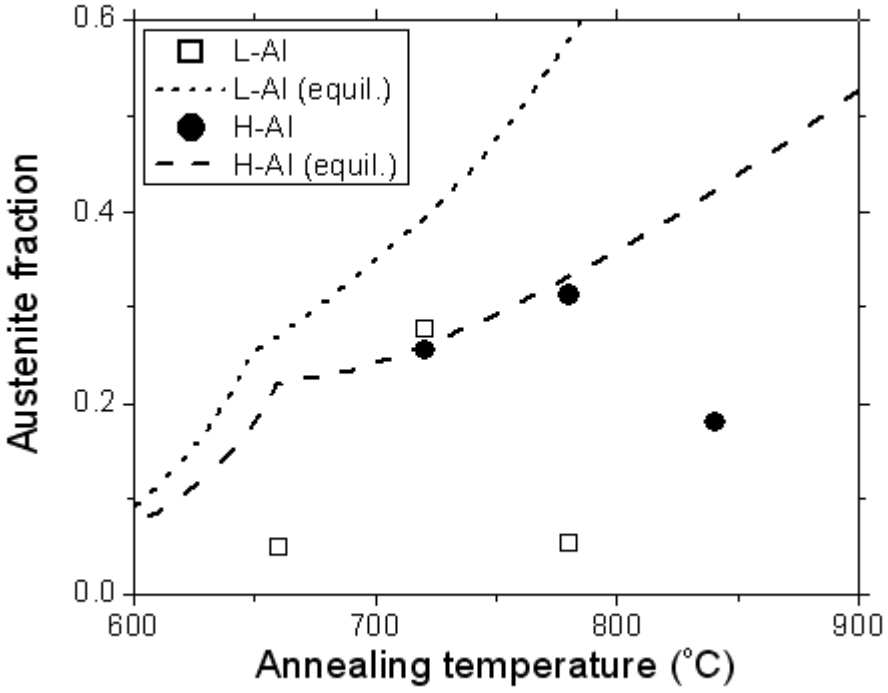
L-Al
L-Al (equil.)
H-Al
H-Al (equil.)
Austenite fraction
0.0
0.2
0.4
0.6
600
700
800
900
Annealing temperature (°C)

Fig. 5

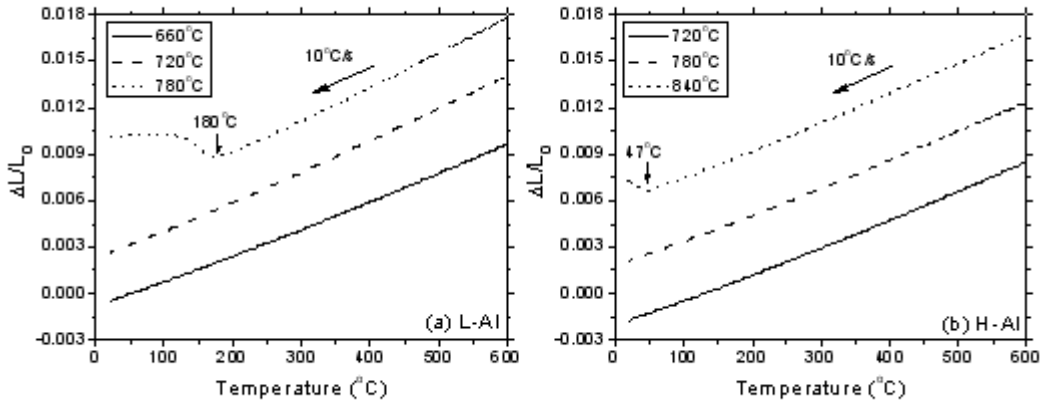
660°C
720°C
780°C
10°C/s
180°C
(a) L-Al
ΔL/L0
Temperature (°C)
720°C
780°C
840°C
10°C/s
47°C
(b) H-Al
ΔL/L0
Temperature (°C)

Fig. 6

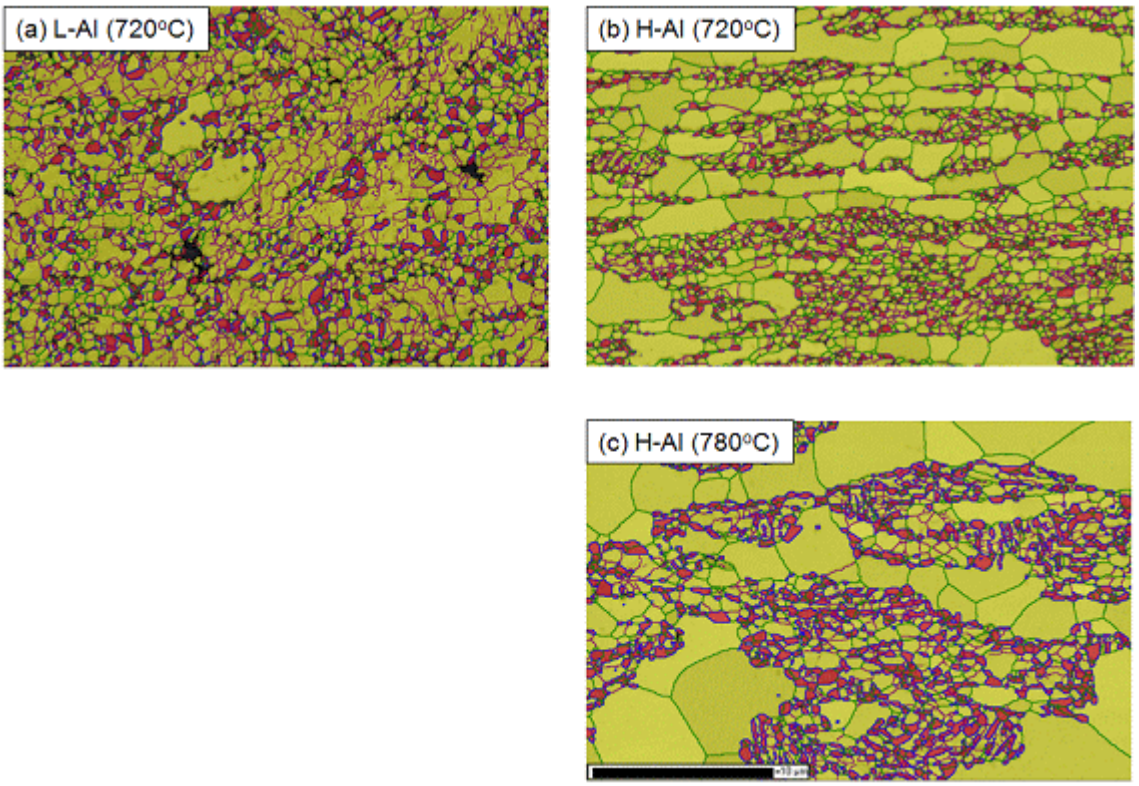

Fig. 7

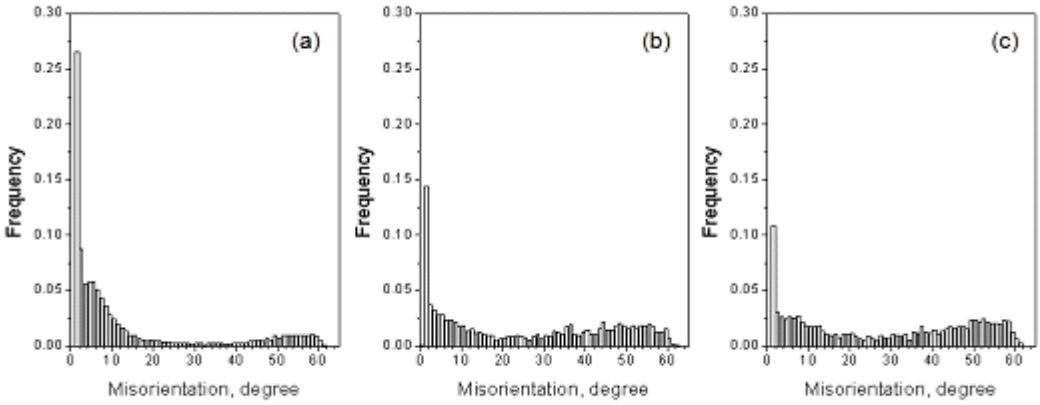
(a)
(b)
(c)
Frequency
Misorientation, degree
0.00
0.05
0.10
0.15
0.20
0.25
0.30
0
10
20
30
40
50
60

Fig. 8

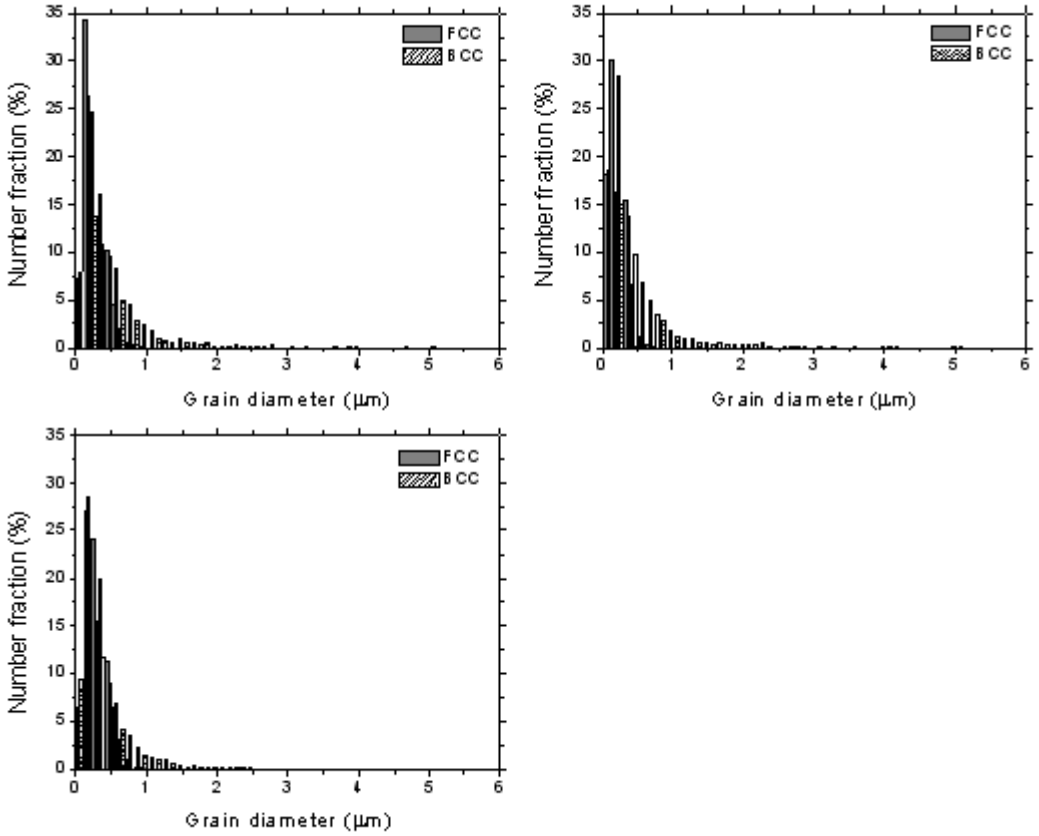
FCC
BCC
Number fraction (%)
Grain diameter (μm)
0
5
10
15
20
25
30
35
0
1
2
3
4
5
6

Fig. 9

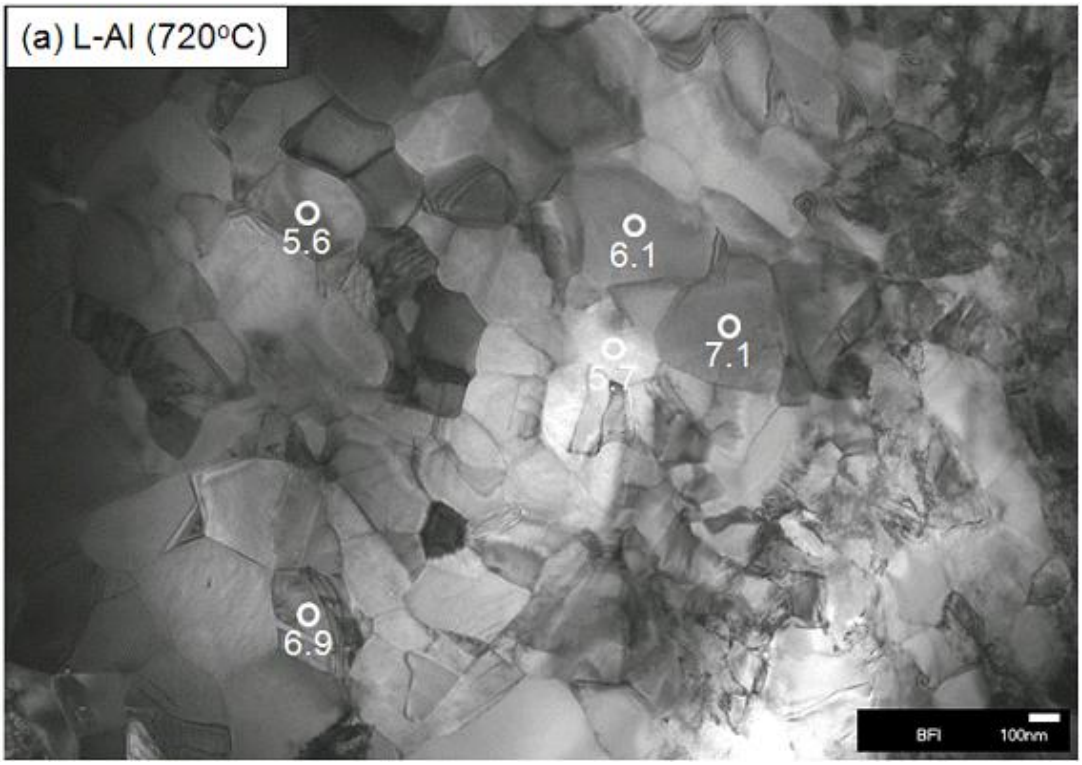

Fig. 10 (a)

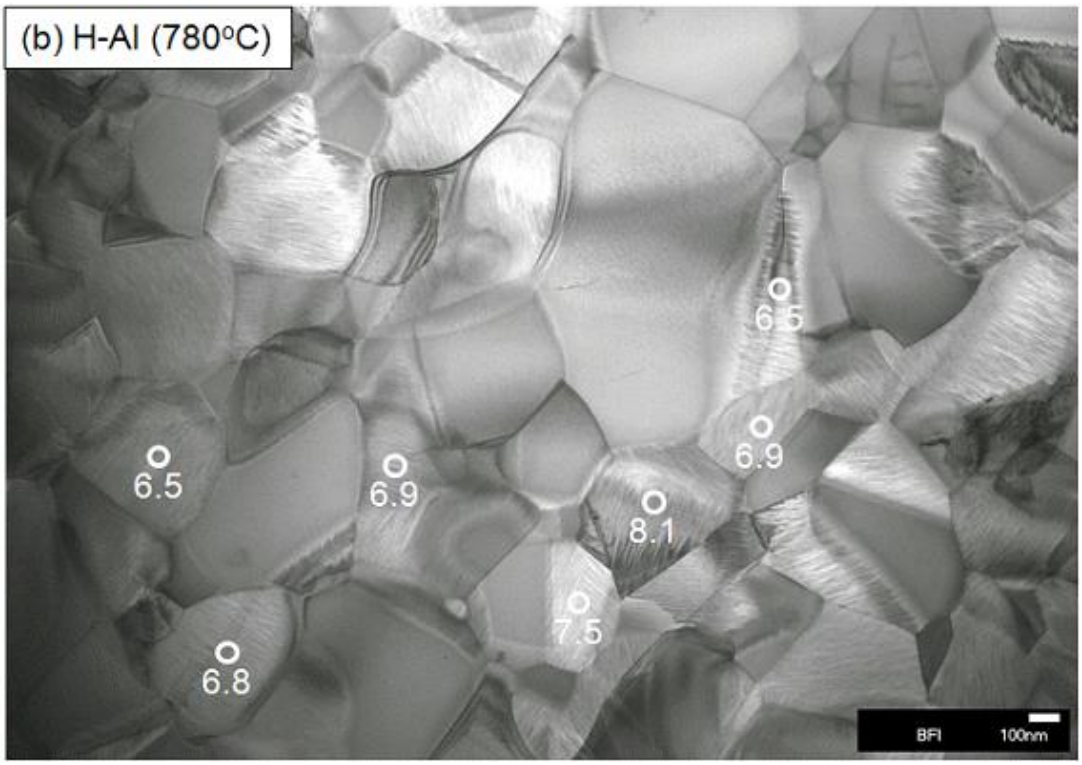

Fig. 10 (b)

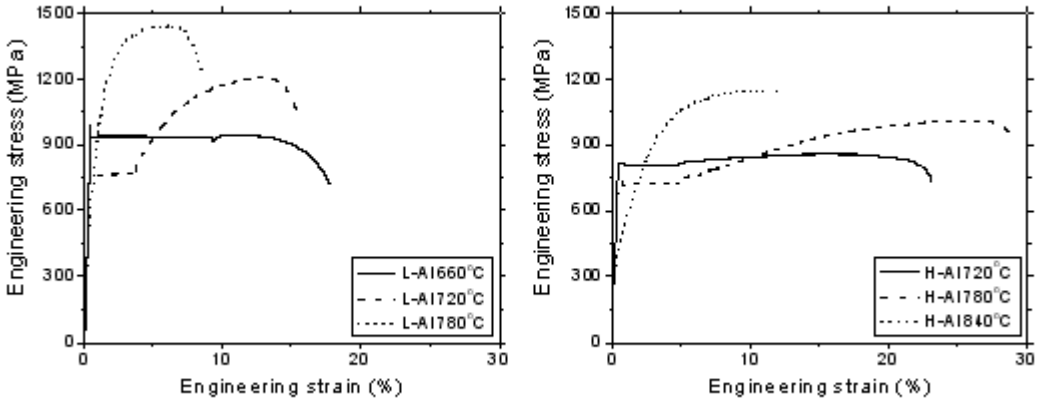
Engineering stress (MPa)
Engineering strain (%)
L-AI660°C
L-AI720°C
L-AI780°C
H-AI720°C
H-AI780°C
H-AI840°C

Fig. 11

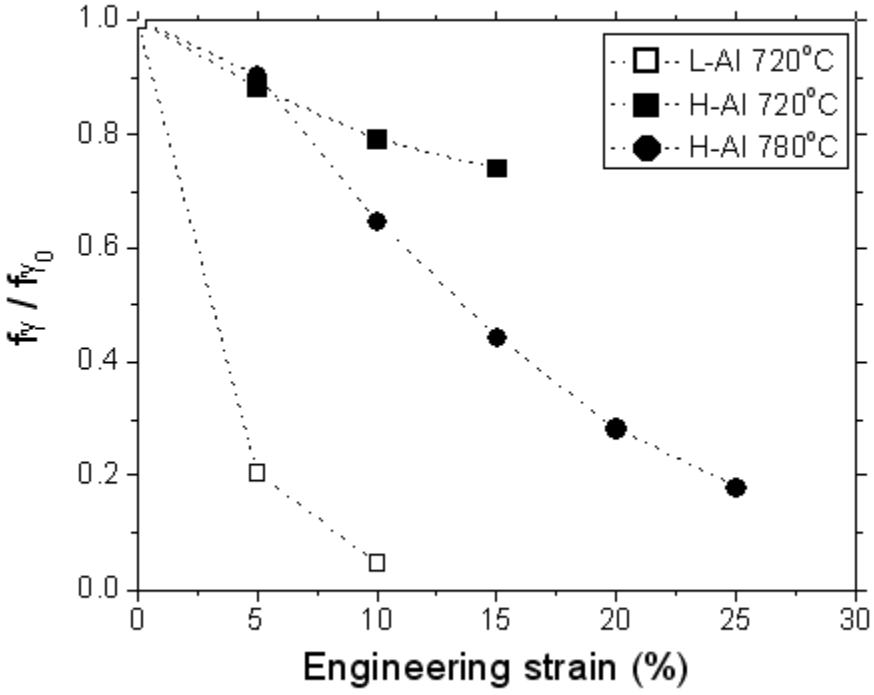
L-Al 720°C
H-Al 720°C
H-Al 780°C
f_γ / f_{γ_0}
Engineering strain (%)
0.0
0.2
0.4
0.6
0.8
1.0
0
5
10
15
20
25
30

Fig. 12